Journal of Alloys and Compounds 620 (2015) 383–389

Contents lists available at ScienceDirect

Journal of Alloys and Compounds

journal homepage: www.elsevier.com/locate/jalcom

Synthesis and luminescence properties of 1,3,4-oxadiazole acetamide derivatives and their rare earth complexes

Wu Zhang [a], Wei He [a], Xiaorui Guo [a], Yanwen Chen [b], Limin Wu [a], Dongcai Guo [a,*]

[a] School of Chemistry and Chemical Engineering, Hunan University, Changsha 410082, China
[b] Institute of Nonferrous Metallurgy Labor Protection, Hunan, Changsha 410014, China

ARTICLE INFO

Article history:
Received 20 February 2014
Accepted 20 September 2014
Available online 13 October 2014

Keywords:
1,3,4-Oxadiazole
Synthesis
Rare earth complexes
Fluorescence properties
Electrochemical properties

ABSTRACT

A series of 1,3,4-oxadiazole acetamide derivatives have been designed and synthesized, and their complexes with Eu(III) and Tb(III) were also prepared. The luminescence properties of the target complexes were investigated, and the results indicated that all target complexes showed the characteristic luminescence of the central ions. The relative fluorescence intensities of the complexes with Eu(III) are higher than that of the complexes with Tb(III). The fluorescence quantum yields of the target complexes were calculated by the reference method, and the results showed that the complexes substituted by electron-donating group possess higher fluorescence quantum yields, compared with that of the complex without substituent, while the complexes substituted by electron-withdrawing group possess lower fluorescence quantum yields. The electrochemical properties of the target complexes were investigated by cyclic voltammetry, the HOMO energy levels of the target complexes substituted by electron-donating group are higher than that of the target complexes substituted by electron-withdrawing group.

1. Introduction

Because of the unique properties, the complexes of rare-earth elements with 1,3,4-oxadiazole and some of derivatives have drawn great attention among scholars. Along with in-depth studies, their application value has also attracted great attention in fluorescent materials, luminescent probes in bio-medical assays and emitters in electroluminescent (EL) devices [1]. In recent years, the design and synthesis of rare earth functional coordination compounds has been one of the researching hot points in the coordination chemistry field [2,3]. The luminescence intensities of rare earth complexes is relationship to the absorption efficiency of ligands, which is dependent on the ligand molecule with expanded π-conjugated system to shift the excitation band of its rare earth complex to visible region. But if expanded π-conjugated system is too small, it will not absorb ultraviolet-light, if is too big, it will not sensitize the rare earth ion to emit characteristic emission [4,5]. In this regard, much attention has been focused on the selecting of ligands with different structure [6]. In general, the architectures of such supramolecule net-works are built-up using multidentate organic ligands containing O- and/or N-donors [7]. In this paper, we choose 1,3,4-oxadiazole acetamide derivatives as chelating ligand, which has a rigid framework and can construct stable supramolecule structures via C—H···O or C—H···N hydrogen bonds and π–π stacks, their corresponding rare earth complexes which possess good stability, fine luminescent monochromaticity and strong fluorescence intensities [8,9]. Based on the above considerations, four novel 1,3,4-oxadiazole acetamide derivatives were designed and synthesized, and their corresponding Tb(III) and Eu(III) complexes were also prepared. The relationship between the structure of ligands and the fluorescence intensities of their rare earth complexes would be studied, meanwhile, the electrochemical properties and fluorescence quantum yields of the target rare earth complexes were discussed in detail. The synthesis route for the 1,3,4-oxadiazole acetamide derivatives ($\mathbf{L^{1-4}}$) is shown in Scheme 1.

2. Experimental

2.1. Materials and methods

Tb_2O_3 (purity 99.99%) and Eu_2O_3 (purity 99.99%) were purchased from commercial suppliers. $Eu(NO_3)_3$ (0.1 mol L^{-1}) and $Tb(NO_3)_3$ (0.1 mol L^{-1}) ethanol solution was prepared according to the literature [10].

Abbreviations: NMR, nuclear magnetic resonance; UV spectra, ultraviolet spectra; IR, infrared spectra; CV, cyclic voltammetric; EDTA, ethylenediaminetetraacetic acid; HOMO, highest occupied molecular orbital; LUMO, lowest unoccupied molecular orbital.

* Corresponding author. Tel./fax: +86 0731 88821449.
E-mail address: dcguo2001@hnu.edu.cn (D. Guo).

http://dx.doi.org/10.1016/j.jallcom.2014.09.153
0925-8388/

^{1}H NMR spectra was recorded in DMSO-d_6/$CDCl_3$ on Brucker spectrophotometer (400 MHz) with TMS as an internal standard. Mass spectra were measured with the MAT95XP Mass Spectrometer. IR spectra (400–4000 cm^{-1}) were obtained in KBr discs by a PERKIN–ELMER Spectrum One. UV spectra (190–450 nm) were recorded by LabTech UV-2100 spectrophotometer, with DMSO as solvent and reference. Elemental analysis of the complexes was carried out on a VarioEL 111 CHNS analyzer. Melting points of all compounds were determined on an X-4 binocular microscope. Thermal gravimetric analysis were carried out on a NETZSCH STA 409PC thermal gravimetric analyzer. Cyclic voltammetry curve testing using three electrodes were glassy electrode, a platinum electrode and a saturated calomel electrode, ferrocene as external standard, nitrite solution was used as the supporting electrolyte and dimethyl sulfoxide as the solvent, the test scanning speed was 100 mV s^{-1} and the sensitivity was 1 mA. The fluorescence spectra were measured by using powder samples on a Hitachi F-2700 Fluorescence Spectrophotometer at room temperature.

2.2. General procedure for synthesis of the intermediates

2.2.1. Synthesis of the compound *A*

The polyphosphate (15 mmol, 5.07 g) was added into a 150 mL three-neck flask and maintained the temperature at 50 °C for some time, and then a solution of hydrazine hydrate (80%, 6.5 mL) and salicylic acid (10 mmol, 1.38 g) was added with stirring. The reaction mixture was heated to 130 °C and refluxed for 7 h with stirring in the oil bath. After completion of the reaction, the resulting mixture was poured into the 500 mL cold water and standed over night with stirring. Then filtered and washed with water, evaporated to obtained the crude product, the compound **A** was obtained by recrystallization from the absolute ethanol. Yield, 76% [11].

2.2.2. Synthesis of the compound B^{1-4}

As the synthesis methods of the compounds $\mathbf{B^{1-4}}$ were similar, only synthesis of the 2-chloro-N-phenylacetamide compound $\mathbf{B^1}$ was described. A solution of aniline (66 mmol, 6.14 g) in glacial acetic acid (50 mL) was added into a 100 mL single-neck flask and then the acetyl chloride (74 mmol, 8.36 g) was gradually dropwise added under stirring in the ice water bath. The resulting reaction mixture was stirred for 1 h at room temperature and then poured into 300 mL saturated sodium acetate solution. Filtered off and washed several times with cold water. The compound $\mathbf{B^1}$ was obtained by recrystallization from the mixture of ethanol and water (1:1) and dried in vacuum for 12 h.

2-chloro-N-phenylacetamide (B^1). White crystals, yield (81%). ^{1}H NMR (400 MHz, DMSO) δ/ppm: 10.29 (s, 1H, NH), 7.77–7.47 (m, 2H, ArH), 7.40–7.22 (m, 2H, ArH), 7.18–6.95 (m, 1H, ArH), 4.25 (s, 2H, CH_2); MS (EI) *m*/*z* (%): 172 (M + 3, 3), 171 (M + 2, 25), 169 (M, 80), 121 (3), 120 (40), 106 (7), 94 (10), 93 (100), 77 (22), 65 (28).

2-chloro-N-*p*-tolylacetamide (B^2). White crystals, yield (75%). ^{1}H NMR (400 MHz, DMSO-d_6) δ/ppm: 10.21 (s, 1H, NH), 7.42–7.46 (m, 2H, ArH), 7.16–7.18 (m, 2H, ArH), 4.22 (s, 2H, CH_2), 2.21 (s, 3H, CH_3); MS (EI) *m*/*z* (%): 186 (M + 3, 3), 185 (M + 2, 25), 183 (M, 75), 148 (4), 134 (27), 107 (100), 106 (76), 91 (16), 77 (26), 51 (10).

2-chloro-N-(4-methoxyphenyl)acetamide (B^3). White crystals, yield (87%). ^{1}H NMR (400 MHz, DMSO-d_6) δ/ppm: ^{1}H NMR (400 MHz, DMSO) δ/ppm: 10.43 (s, 1H, NH), 7.67–7.57 (m, 2H, ArH), 7.46–7.34 (m, 2H, ArH), 4.26 (s, 2H, CH_2); MS (EI) *m*/*z* (%): 207 (M + 3, 5), 205 (M + 1, 33), 203 (M-1, 52), 156 (4), 154 (13), 129 (32), 127 (100), 126 (15), 111 (5), 99 (14), 77 (5), 63 (7).

2-chloro-N-(4-chlorophenyl)acetamide (B^4). Yellow crystals, yield (85%). ^{1}H NMR (400 MHz, DMSO) δ/ppm: 10.18 (s, 1H, NH), 7.54–7.48 (m, 2H, ArH), 6.95–6.87 (m, 2H, ArH), 4.22 (s, 2H, CH_2), 3.73 (s, 3H, CH_3); MS (EI) *m*/*z* (%): 202 (M + 3, 3), 201 (M + 2, 32), 199 (M, 100), 124 (29), 123 (72), 108 (72), 95 (13), 80 (6).

2.3. General procedure for synthesis of the target compound (L^{1-4})

As the synthesis methods of compounds $\mathbf{L^{1-4}}$ were similar, the synthesis of the target compound $\mathbf{L^1}$ was described as an example., the 2,2′-(1,3,4-oxadiazole-2,5-diyl)diphenol (2 mmol, 0.51 g) and anhydrous potassium carbonate (10 mmol, 1.38 g) were dissolved in a 100 mL single-necked flask with 50 mL DMF solution. The resulting mixture was refluxed at 80 °C for 1 h, the 2-chloro-N-phenylacetamide compound $\mathbf{B^1}$ (7 mmol, 1.18 g) and a little of KI were added and continued to reflux for 24 h. After completion of the reaction, the reaction mixture was cooled to room temperature, and then gradually poured into distilled water (500 mL) and stirred for 2 h. The resulting mixture was concentrated under reduced pressure and washed several times with distilled water until the pH value reached 7. The resulting product was further purified by recrystallization from the mixture of ethanol and chloroform (1:1), and dried in vacuum for 24 h. Thus the target compound $\mathbf{L^1}$ was obtained.

2,2′-(2,2′-(1,3,4-oxadiazole-2,5-diyl)bis(2,1-phenylene))bis(oxy)bis(N-phenylacetamide) (L^1). White powder, yield (84%). m.p. 265–266 °C; ^{1}H NMR (400 MHz, $CDCl_3$) δ/ppm: 10.55 (s, 2H, NH), 8.10 (dd, *J* = 7.8, J = 1.6 Hz, 2H, ArH), 7.73–7.68 (m, 4H, ArH), 7.65–7.59 (m, 2H, ArH), 7.26–7.22 (m, 2H, ArH), 7.13 (d, *J* = 8.2 Hz, 2H, ArH), 7.06 (dd, *J* = 10.8 Hz, *J* = 5.1 Hz, 4H, ArH), 6.86 (t, *J* = 7.4 Hz, 2H, ArH), 4.85 (s, 4H, CH_2); IR (KBr) v/cm^{-1}: 3306, 3020, 1759, 1692, 1601, 1255, 1165, 866; MS (EI) *m*/*z* (%): 522 (M + 2, 2), 520 (M, 4), 311 (100), 254 (78), 226 (18), 121 (47), 106 (24), 93 (51); Anal. Calcd. for $C_{30}H_{24}N_4O_5$: C, 69.22; H, 4.65; N, 10.76. Found: C, 69.21; H, 4.55; N, 10.56.

2,2′-(2,2′-(1,3,4-oxadiazole-2,5-diyl)bis(2,1-phenylene))bis(oxy)bis(N-p-tolylacetamide) (L^2). Yellow crystals, yield (71%). m.p. 259–260 °C; ^{1}H NMR (400 MHz, $CDCl_3$) δ/ppm: 10.45 (s, 2H, NH), 8.10 (dd, *J* = 7.8 Hz, *J* = 1.6 Hz, 2H, ArH), 7.64–7.59 (m, 2H, ArH), 7.53 (d, *J* = 8.4 Hz, 4H, ArH), 7.23 (d, *J* = 7.8 Hz, 2H, ArH), 7.12 (d, *J* = 8.3 Hz, 2H, ArH), 6.81 (d, *J* = 8.2 Hz, 4H, ArH), 4.82 (s, 4H, CH_2), 2.12 (s, 6H, CH_3); IR (KBr) v/cm^{-1}: 3325, 3132, 2151, 1680, 1600, 1268, 1166, 866; MS (EI) *m*/*z* (%): 550 (M + 2, 8), 549 (M + 1, 37), 548 (M, 100), 442 (97), 443 (26), 415 (61), 268 (72), 121 (44); Anal. Calcd. for $C_{32}H_{28}N_4O_5$: C, 70.06; H, 5.14; N, 10.21. Found: C, 70.04; H, 5.12; N, 10.11.

2,2′-(2,2′-(1,3,4-oxadiazole-2,5-diyl)bis(2,1-phenylene))bis(oxy)bis(N-(4-methoxyphenyl)acetamide) (L^3). White powder, yield (70%). m.p. 225–226 °C; 1H NMR (400 MHz, $CDCl_3$) δ/ppm: δ 10.45 (s, 2H, NH), 8.13–8.08 (m, 2H, ArH), 7.64–7.56 (m, 6H, ArH), 7.24 (d, *J* = 7.6 Hz, 2H, ArH), 7.13 (d, *J* = 8.3 Hz, 2H, ArH), 6.57 (d, *J* = 8.9 Hz, 4H, ArH), 4.83 (s, 4H, CH2), 3.66 (s, 6H, CH3O); IR (KBr) v/cm^{-1}: 3229, 3132, 1964, 1735, 1671, 1250, 1162, 964; MS (EI) *m*/*z* (%): 582 (M + 2, 3), 581 (M + 1, 12), 580 (M, 31), 458 (27), 300 (29), 283 (46), 136 (47), 123 (100), 121 (72), 108 (59); Anal. Calcd. for $C_{32}H_{28}N_4O_7$: C, 66.20; H, 4.86; N, 9.65; O 19.29. Found: C, 66.12; H, 4.62; N, 9.55.

2,2′-(2,2′-(1,3,4-oxadiazole-2,5-diyl)bis(2,1-phenylene))bis(oxy)bis(N-(4-chlorophenyl)acetamide) (L^4). Yellow crystals, yield (74%). m.p. 288–289 °C; ^{1}H NMR (400 MHz, $CDCl_3$) δ/ppm: 10.68 (s, 2H, NH), 8.14 (dd, *J* = 7.8 Hz, *J* = 1.5 Hz, 2H, ArH), 7.67–7.63 (m, 2H, ArH), 7.56 (d, *J* = 8.8 Hz, 4H, ArH), 7.28 (d, *J* = 7.5 Hz, 2H, ArH), 7.13 (d, *J* = 8.3 Hz, 2H, ArH), 6.99–6.95 (m, 4H, ArH), 4.85 (s, 4H, CH_2); IR (KBr) v/cm^{-1}: 3223, 3040, 1879, 1691, 1604, 1267, 1164, 868; MS (EI) *m*/*z* (%): 592 (M + 4, 7), 591 (M + 3, 12), 590 (M + 2, 38), 589 (M + 1, 17), 588 (M, 56), 462 (97), 435 (86), 288 (60), 148 (57), 121 (100); Anal. Calcd. for $C_{30}H_{22}N_4O_5Cl_2$: C, 61.13; H, 3.76; N, 9.51. Found: C, 61.10; H, 3.56; N, 9.42.

2.4. Synthesis of the target rare earth complexes

The synthesis methods of the target rare earth complexes were similar, the synthesis of the europium complexes of compound $\mathbf{L^1}$ was described as an example. A mixture of compound $\mathbf{L^1}$ (0.40 mmol), chloroform (40 mL) was added into a 100 mL

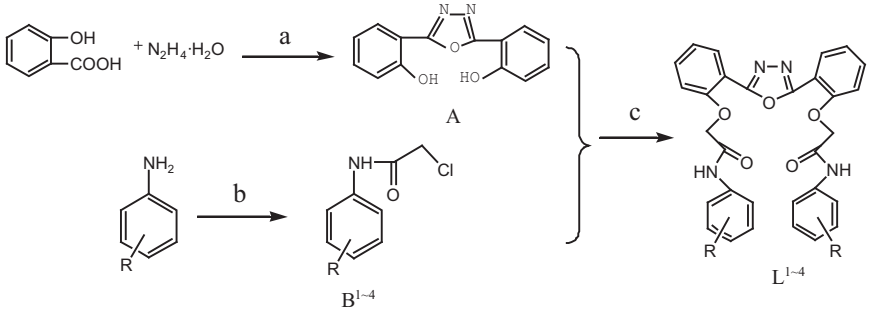

B^1, R=4-H; B^2, R=4-CH_3; B^3, R=4-CH_3O; B^4, R=4-Cl

L^1, R=4-H; L^2, R=4-CH_3; L^3, R=4-CH_3O; L^4, R=4-Cl

(a) $H_6P_4O_{13}$, reflux, 7 h; (b) $ClCH_2COCl$, CH_3COOH, r.t., 1.5 h; (c) DMF, K_2CO_3, KI, reflux, 24 h

Scheme 1. The synthesis route for the ligands $\mathbf{L^{1-4}}$.

three-neck flask and refluxed at 60 °C for some time, and then 4 mL $Eu(NO_3)_3$ (0.1 mol L^{-1}) ethanol solution was added. The pH value of the reaction mixture was adjusted to 6.5 with sodium ethoxide, a large number of precipitate was formed, and then laid aside at room temperature for 3 h. The product was washed several times with chloroform, filtered and dried in vacuum for 12 h.

3. Results and discussion

3.1. Element analysis and solubility of the target complexes

The molar conductance data, element analysis data (C, H and N) and total rare earth element contents of the target complexes are shown in Table 1.

It is seen from Table 1 that the experimental data are in good agreement with the theoretical values, which indicates that the composition of the target complexes are $RE(NO_3)_3L^{1-4} \cdot 2H_2O$. The molar conductivity values of the target complexes in acetone solution are in the range of 7–15 S cm^2 mol^{-1}, which reveals that the target complexes are non-electrolytes [12], this result indicates that there are three nitrate ligands participate into coordination.

The ligands $\mathbf{L^{1-4}}$ are very soluble in chloroform, DMF and DMSO, and soluble in ethanol and acetone, but insoluble in water, cyclohexane, benzene and so on. While the target complexes are soluble in DMF and DMSO, but insoluble in ethanol, cyclohexane, benzene and so on.

3.2. UV spectra analysis

The UV spectra of the ligands $\mathbf{L^{1-4}}$ and their corresponding target complexes were recorded in DMSO solution, and the data are summarized in Table 2. Since the UV spectra of all ligands and their target complexes are similar, the UV spectra of the ligands $\mathbf{L^1}$ and $\mathbf{L^2}$ as well as their complexes $Tb(NO_3)_3L^1 \cdot 2H_2O$ and $Eu(NO_3)_3L^2 \cdot 2H_2O$ are selected for illustration and shown in Figs. 1 and 2, respectively.

It is shown from Table 2 that all free ligands $\pi \rightarrow \pi^*$ transitions absorption band are in the range of 259–262 nm, $n \rightarrow \pi^*$ transitions absorption band in the range of 315–317 nm. The Fig. 1 shows two absorption peaks at 259 nm and 315 nm, which are ascribed to the π–π^* and n–π^* transitions in the ligand $\mathbf{L^1}$, respectively, while, the profile of absorption spectrum of the $Tb(NO_3)_3L^1 \cdot 2H_2O$ has changed comparing to the free ligand $\mathbf{L^1}$ [13], this result shows that the $\mathbf{L^1}$ takes part in coordination with central ion. The Fig. 2 shows that the UV absorption spectrum of the $Eu(NO_3)_3L^2 \cdot 2H_2O$, it shows $n \rightarrow \pi^*$ transitions absorption peak at 317 nm, while the band for the ligand $\mathbf{L^2}$ is about 318 nm, this phenomenon can be explained by the expansion π-conjugated system that caused by the central ion coordination.

3.3. Infrared spectra analysis

The IR spectra data of all ligands and their corresponding rare earth complexes are presented in the Table 3. IR spectra of all

Table 2
UV spectra data of the target complexes.

Complexes	λ_{max} (nm)	Ligand	λ_{max} (nm)
$Eu(NO_3)_3L^1 \cdot 2H_2O$	259, 317	L^1	259, 315
$Eu(NO_3)_3L^2 \cdot 2H_2O$	261, 318	L^2	261, 317
$Eu(NO_3)_3L^3 \cdot 2H_2O$	262, 318	L^3	261, 317
$Eu(NO_3)_3L^4 \cdot 2H_2O$	262, 317	L^4	262, 316
$Tb(NO_3)_3L^1 \cdot 2H_2O$	259,317	L^1	259, 315
$Tb(NO_3)_3L^2 \cdot 2H_2O$	260, 318	L^2	261, 317
$Tb(NO_3)_3L^3 \cdot 2H_2O$	263,316	L^3	261, 317
$Tb(NO_3)_3L^4 \cdot 2H_2O$	262, 317	L^4	262, 316

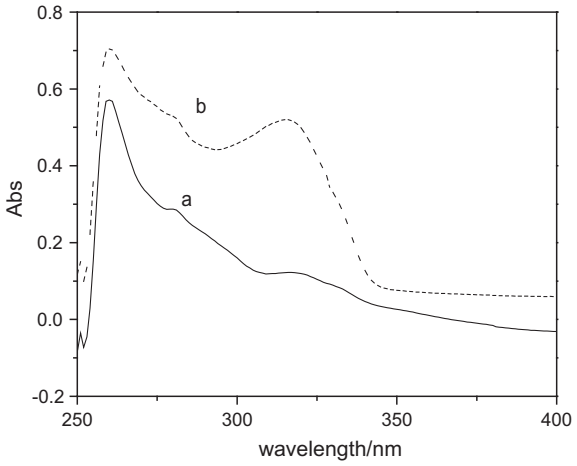

Fig. 1. UV spectra of the $Tb(NO_3)_3\mathbf{L^1} \cdot 2H_2O$ (a) and the ligand $\mathbf{L^1}$(b).

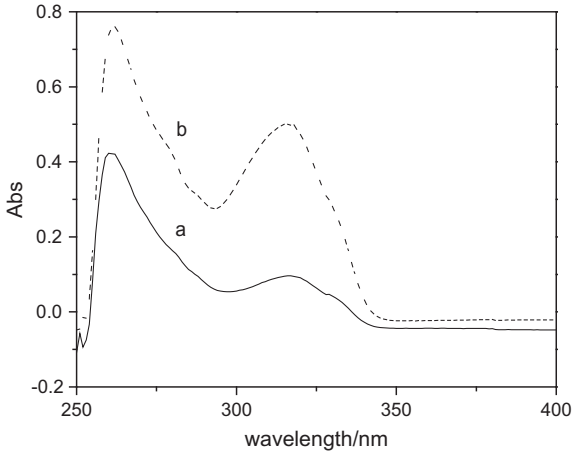

Fig. 2. UV spectra of the $Eu(NO_3)_3\mathbf{L^2} \cdot 2H_2O$ (a) and the ligand $\mathbf{L^2}$(b).

Table 1
Element analysis and molar conductance data of the target complexes.

Complexes	Found (calculated) (%)				Λ_m
	C	H	N	RE	(S cm^2 mol^{-1})
$Eu(NO_3)_3L^1 \cdot 2H_2O$	40.15 (40.28)	3.17 (3.15)	10.68 (10.96)	17.02 (16.99)	8
$Eu(NO_3)_3L^2 \cdot 2H_2O$	41.54 (41.66)	3.33 (3.50)	9.52 (10.63)	16.98 (16.47)	12
$Eu(NO_3)_3L^3 \cdot 2H_2O$	39.99 (40.26)	3.57 (3.38)	10.04 (10.27)	15.87 (15.92)	14
$Eu(NO_3)_3L^4 \cdot 2H_2O$	37.58 (37.40)	2.56 (2.72)	10.69 (10.18)	16.12 (15.77)	7
$Tb(NO_3)_3L^1 \cdot 2H_2O$	39.77 (39.97)	3.19 (3.13)	11.20 (10.88)	17.58 (17.63)	15
$Tb(NO_3)_3L^2 \cdot 2H_2O$	41.56 (41.35)	3.36 (3.47)	10.52 (10.55)	16.75 (17.10)	10
$Tb(NO_3)_3L^3 \cdot 2H_2O$	39.99 (39.97)	3.47 (3.35)	10.08 (10.20)	16.36 (16.53)	8
$Tb(NO_3)_3L^4 \cdot 2H_2O$	36.87 (37.13)	2.54 (2.70)	9.89 (10.10)	16.85 (16.38)	12

Table 3
Infrared spectra data of the ligands and their corresponding target complexes.

Compound	$\upsilon_{C=O}$	$\upsilon_{C=N}$	υ_{C-O-C}	υ_{Ar-O-C}	υ_{NO3}^{-} ν_1	ν_2	ν_3	ν_4	$\lvert\nu_1-\nu_4\rvert$
L^1	1692	1601	1165	1255					
$Eu(NO_3)_3L^1 \cdot 2H_2O$	1632	1600	1167	1255	1498	1031	814	1345	153
$Tb(NO_3)_3L^1 \cdot 2H_2O$	1691	1602	1167	1255	1486	1043	835	1349	137
L^2	1680	1600	1166	1268					
$Eu(NO_3)_3L^2 \cdot 2H_2O$	1667	1600	1163	1265	1494	1026	811	1298	196
$Tb(NO_3)_3L^2 \cdot 2H_2O$	1665	1603	1164	1265	1496	1041	835	1301	195
L^3	1671	1605	1162	1250					
$Eu(NO_3)_3L^3 \cdot 2H_2O$	1656	1605	1161	1248	1494	1029	827	1300	194
$Tb(NO_3)_3L^3 \cdot 2H_2O$	1655	1606	1163	1248	1498	1033	830	1301	197
L^4	1691	1604	1163	1267					
$Eu(NO_3)_3L^4 \cdot 2H_2O$	1689	1604	1164	1267	1496	1038	820	1329	167
$Tb(NO_3)_3L^4 \cdot 2H_2O$	1688	1603	1164	1267	1496	1038	834	1314	185

target complexes show the similar features. It reveals that the coordination types of the complexes are similar [14], the IR spectra of ligand **L¹** as well as their corresponding complex $Eu(NO_3)_3L^1 \cdot 2H_2O$ is selected for illustration and shown in Fig. 3.

As shown in the Table 3 and Fig. 3, the band at 1692 cm^{-1} for the free ligand **L¹** is assigned to the ν(C=O) stretch, which shifts to 1632 cm^{-1} for its complex $Eu(NO_3)_3L^1 \cdot 2H_2O$, which confirms that the oxygen atom of the amide group bonds to the rare earth ions. In addition, the IR spectra of the ligand **L¹** shows the characteristic absorption peaks of the C=N group at 1601 cm^{-1} and Ar—O—C group stretching modes at 1259 cm^{-1}, while, those bands are not obviously shifted in its corresponding complex $Eu(NO_3)_3L^1 \cdot 2H_2O$, which confirms that the nitrogen of C=N group and oxygen of Ar—O—C group hardly participate into coordination, this phenomenon is ascribed to the sterically hindered occurring. In the target complexes, the absorption bands of the coordinated nitrates are observed at 1498 (ν_{as}) and 1345 (ν_s) cm^{-1}, but there is not characteristic absorption peak of free nitrates at 1385 cm^{-1}, which is agreement with the result of the conductivity experiments, this result clearly shows that the nitrate groups participate in coordination with rare earth ions successfully. In addition, the separation of the two highest frequency bands $|\nu_1-\nu_4|$ is approximately 153 cm^{-1}, indicating that the coordinated nitrate groups in the complexes are bidentate [15].

3.4. Thermal analysis

In order to investigate the thermal decomposition of the target complexes, the thermal analysis was carried out. The eight target complexes present similar thermal behaviors, in this paper, we only give the TG and DSC curves of $Eu(NO_3)_3L^2 \cdot 2H_2O$ for illustration and shown in Fig. 4. The thermogravimetric analysis data was summarized in Table 4.

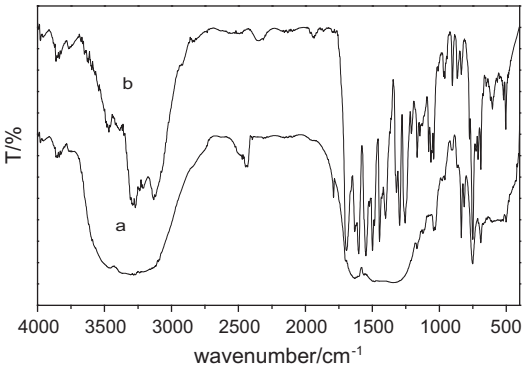

Fig. 3. IR spectra of $Eu(NO_3)_3L^1 \cdot 2H_2O$ (a) and **L¹**(b).

The Fig. 4 shows that the weight losses of the first step for them is 3.35% between 70 and 200 °C, these values are well agreement with the loss of two lattice water molecules depending on the target complexes, the calculated value is 3.90%. In addition, the TG and DSC of complexes are without endothermic peak and weightlessness at 200–230 °C, which illustrates that the water do not participate into coordination, because the coordination water of the analogous complexes is usually released over 200 °C. And then, there are two remarkable weight loss stages in the TG curve. The one loss stage ranged from 250 to 450 °C was attributed to the decomposition of the ligand **L²**, the experimental value (56.64%) is coincided with the theoretical value (57.37%), meanthile, this result is consistent with the exothermic peak at 443 °C in the DSC curve. The another loss stage of the complex appeared within 450–650 °C is due to the weight loss of three nitrate radical (weight loss, 18.92%. Calcd., 19.17%), and accompanied by a very strong exothermic peak in the DSC curve at 553 °C [16]. The target complex $Eu(NO_3)_3L^2 \cdot 2H_2O$ is decomposed completely at approaching 650 °C, and the remained solid composition is Eu_2O_3

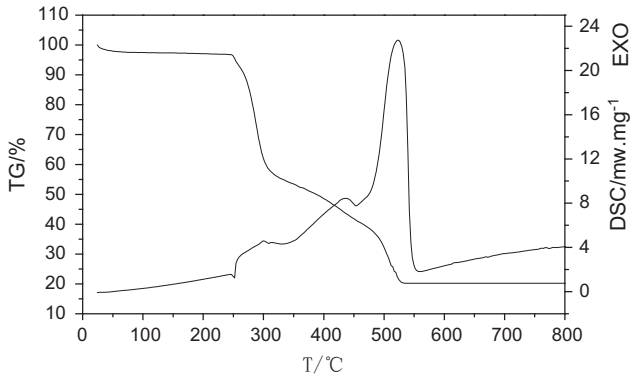

Fig. 4. TG–DSC curves of $Eu(NO_3)_3L^2 \cdot 2H_2O$.

Table 4
Thermal analysis data for target complexes.

Complexes	Endothermic peak (°C)	Exothermic peak (°C)	Metal residue (%)
$Eu(NO_3)_3L^1 \cdot 2H_2O$	287	345, 486,618	25.68 (19.74)
$Eu(NO_3)_3L^2 \cdot 2H_2O$	256	301, 443, 553	20.63 (20.18)
$Eu(NO_3)_3L^3 \cdot 2H_2O$	235	386, 415,565	20.14 (18.48)
$Eu(NO_3)_3L^4 \cdot 2H_2O$	242	326,438 ,578	18.53 (18.33)
$Tb(NO_3)_3L^1 \cdot 2H_2O$	306	342,433, 619,	26.12 (20.72)
$Tb(NO_3)_3L^2 \cdot 2H_2O$	214	324,417, 560	20.78 (20.16)
$Tb(NO_3)_3L^3 \cdot 2H_2O$	261	382,425,596	18.32 (19.43)
$Tb(NO_3)_3L^4 \cdot 2H_2O$	291	338,478,580	28.64 (27.25)

and its quality percentage is 28.64%, which is identical to the calculated value 27.25%. The thermal analysis results show that the target complexes have relatively high thermal stability, and are consistent with the results of other analysis results.

3.5. Fluorescence properties analysis

The fluorescence properties of the target complexes were determined on the solid state at room temperature, and their data are summarized in Table 5. The observed fluorescence spectra of all target complexes are similar, so the fluorescence spectra of $Eu(NO_3)_3L^2 \cdot 2H_2O$ and $Tb(NO_3)_3L^2 \cdot 2H_2O$ are selected for illustration, and the excitation and emission spectra of $Eu(NO_3)_3L^2 \cdot 2H_2O$ are shown in Figs. 5 and 6, the excitation and emission spectra of $Tb(NO_3)_3L^2 \cdot 2H_2O$ are shown in Figs. 7 and 8, respectively.

As shown in the Fig. 5, the excitation spectrum of $Eu(NO_3)_3L^2 \cdot 2H_2O$, which was measured under 614 nm emission wavelength, possesses a broad excitation band with the strongest excitation peak at 397 nm. Meanwhile, the Fig. 6 shows that the emission spectra for $Eu(NO_3)_3L^2 \cdot 2H_2O$ are composed of the characteristic emission peaks of Eu (III) arising from $^5D_0 \rightarrow {}^7F_1$ (594 nm), $^5D_0 \rightarrow {}^7F_2$ (620 nm), respectively. It is noted that the intensity ratio of $^5D_0 \rightarrow {}^7F_2$ (electric dipole transition) and $^5D_0 \rightarrow {}^7F_1$ (magnetic dipole transition) is 3.14, which indicates that the Eu(III) ion lies in the asymmetry center [17]. Additionally, there is a narrow and sharp emission peak appearing at approximate 620 nm, and the target europium complexes show the intensely red fluorescence, which indicates that the target complexes have good monochromaticity and the ligands are a comparatively good organic chelator for the absorbtion and transfer of energy to the center ion. The Table 5 showed that the excitation spectra of four Tb(III) complexes were obtained by monitoring their emissions at 548 nm, the maximum peaks was at 331, 354, 364, and 354 nm, respectively. The emission spectra of the $Tb(NO_3)_3L^2 \cdot 2H_2O$ was obtained under the excitation spectrum at 354 nm, the major emission peaks showed at 491, 547, 587, and 624 nm, which are assigned

Table 5
Fluorescence spectra data of the target complexes.

Compound	Slit(nm)	λ_{ex} (nm)	λ_{em} (nm)	RFI	Assignment
L^1	2.5	317	364	396.5	
$Eu(NO_3)_3L^1 \cdot 2H_2O$	2.5	395	594	224.2	$^5D_0$—$^7F_1$
			619	485.6	$^5D_0$—$^7F_2$
$Tb(NO_3)_3L^1 \cdot 2H_2O$	2.5	331	491	426.5	$^5D_4 \rightarrow {}^7F_6$
			546	198.5	$^5D_4 \rightarrow {}^7F_5$
			585	98.5	$^5D_4 \rightarrow {}^7F_4$
			625	37.9	$^5D_4 \rightarrow {}^7F_3$
L^2	2.5	317	366	9998	
$Eu(NO_3)_3L^2 \cdot 2H_2O$	2.5	397	594	383.6	$^5D_0$—$^7F_1$
			620	1307	$^5D_0$—$^7F_2$
$Tb(NO_3)_3L^2 \cdot 2H_2O$	2.5	354	491	552.2	$^5D_4 \rightarrow {}^7F_6$
			547	818.8	$^5D_4 \rightarrow {}^7F_5$
			587	143.2	$^5D_4 \rightarrow {}^7F_4$
			624	64.56	$^5D_4 \rightarrow {}^7F_3$
L^3	2.5	317	377	562.9	
$Eu(NO_3)_3L^3 \cdot 2H_2O$	2.5	395	594	605.2	$^5D_0$—$^7F_1$
			619	1236.6	$^5D_0$—$^7F_2$
$Tb(NO_3)_3L^3 \cdot 2H_2O$	2.5	364	491	368.4	$^5D_4 \rightarrow {}^7F_6$
			546	998.4	$^5D_4 \rightarrow {}^7F_5$
			585	26.2	$^5D_4 \rightarrow {}^7F_4$
			622	79.1	$^5D_4 \rightarrow {}^7F_3$
L^4	2.5	317	376	201	
$Eu(NO_3)_3L^4 \cdot 2H_2O$	2.5	396	594	123.6	$^5D_0$—$^7F_1$
			619	386.4	$^5D_0$—$^7F_2$
$Tb(NO_3)_3L^4 \cdot 2H_2O$	2.5	354	491	264.6	$^5D_4 \rightarrow {}^7F_6$
			545	89.4	$^5D_4 \rightarrow {}^7F_5$
			587	37.2	$^5D_4 \rightarrow {}^7F_4$
			625	32.9	$^5D_4 \rightarrow {}^7F_3$

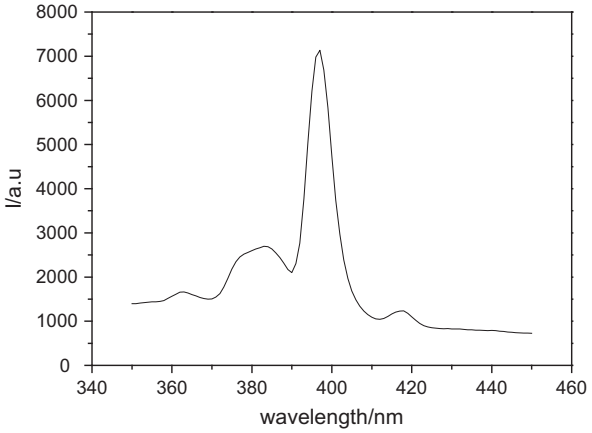

Fig. 5. Excitation spectra of $Eu(NO_3)_3\mathbf{L^2} \cdot 2H_2O$.

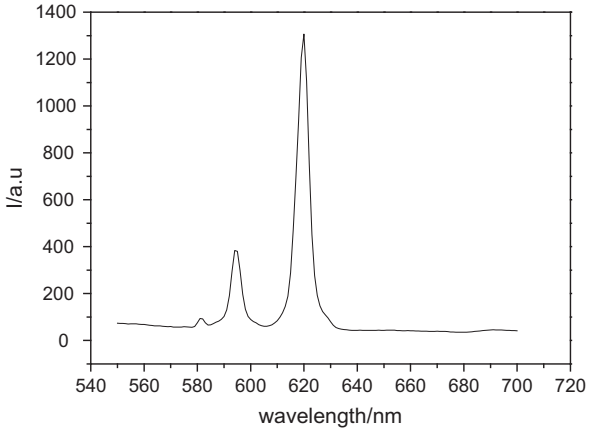

Fig. 6. Emission spectra of $Eu(NO_3)_3\mathbf{L^2} \cdot 2H_2O$.

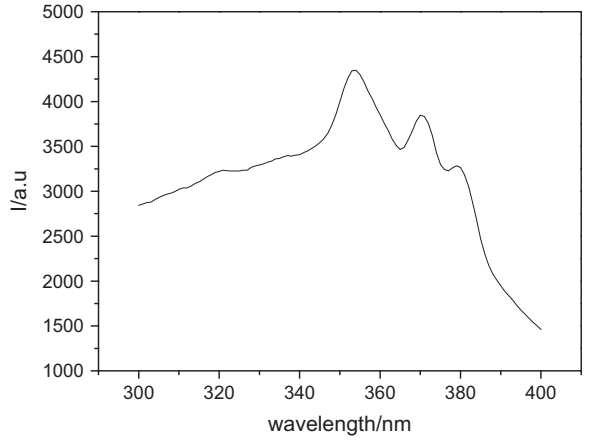

Fig. 7. Excitation spectra of $Tb(NO_3)_3\mathbf{L^2} \cdot 2H_2O$.

to the characteristic emission $^5D_4 \rightarrow {}^7F_J$ ($J = 6, 5, 4, 3$) transitions of Tb^{3+} ion, respectively. This process could be described as follows: the 1,3,4-oxadiazole acetamide ligands were excited to the excited singlet state (S_1) by photon absorption in the UV region, and relaxed to the triplet state (T_1) via intersystem crossing. Then, the energy was nonradiatively transferred from the triplet state of the ligands to a resonance state of the coordinated Tb^{3+} ion. Finally, the Tb^{3+} ion emitted characteristic fluorescence in the visible

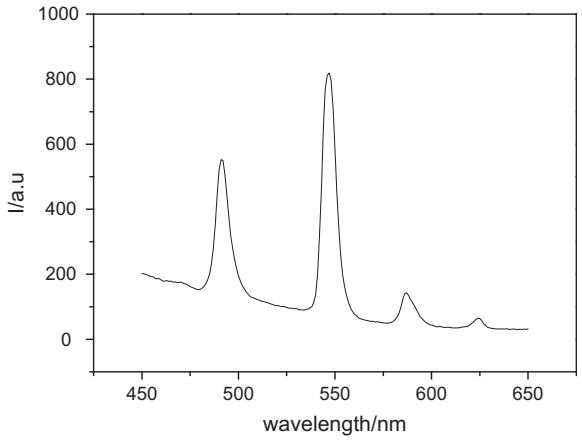

Fig. 8. Emission spectra of $Tb(NO_3)_3\mathbf{L^2} \cdot 2H_2O$.

region by a multi-photon relaxation from the exited state to ground state of Tb^{3+} ion [18].

The Table 5 shows that the fluorescence intensities of complexes $RE(NO_3)_3L^2 \cdot 2H_2O$ were stronger than that of the complexes $RE(NO_3)_3L^1 \cdot 2H_2O$, this was because the ligands $\mathbf{L^2}$ had an donative electron group (—CH_3) which strengthen the molecular rigidity and enlarged the π-conjugated systems of the ligand $\mathbf{L^2}$, so that made $\pi \rightarrow \pi^*$ transition much easier [19]. While the fluorescence intensities of complexes $RE(NO_3)_3L^4 \cdot 2H_2O$ were worse than that of the complexes $RE(NO_3)_3L^1 \cdot 2H_2O$, this phenomenon was ascribed to the ligand $\mathbf{L^4}$ owning the electron-withdrawing group (—Cl) that caused the electron density of the phenyl ring decreasing. The above results showed that the electron-withdrawing groups on the ligands can decrease the fluorescence intensities of their corresponding rare earth complexes, the reasons are that the n–π^* transition of the accepting electron substituent belongs to forbidden transition, the excited state molecules are seldom obtained, and the S^1–T^1 crossing intersystem occupies the dominant position [20]. On the contrary, the electron-donating groups on the ligands are resulted in increasing of the fluorescence intensities of the target complexes, which is owing to the electron-donating groups can induce electronic rearrangement of the target complexes that it can improve the energy level matchment between the ligands and the central rare earth ions, so that the ligands can absorb light energy and transfer it to rare earth ions efficiently. The above results further highlight that the nature of substituents has a great effect upon the fluorescence intensities of the target complexes.

Based on the theory of antenna effect [21]. the fluorescence intensities of the target complexes is related to the efficiency of the intramolecular energy transfer between the triple level of the ligands and the vibrational level of the rare earth ions, which depends on the energy gap between the two levels. It is shown in Table 5 that the fluorescence intensities of $Eu(NO_3)_3L^{1-4} \cdot 2H_2O$ are stronger than that of the $Tb(NO_3)_3L^{1-4} \cdot 2H_2O$, which illustrates that the triple level of ligands matching with the vibrational level of Eu^{3+} are better than that of the Tb^{3+}.

3.6. Fluorescence quantum yields analysis

The fluorescence quantum yields ($\mathbf{\Phi}_{fx}$) are calculated by comparative method [22] using the following equation.

$$\mathbf{\Phi}_{fx} = \frac{n_x^2}{n_{std}^2} \cdot \frac{F_x}{F_{std}} \cdot \frac{A_{std}}{A_x} \cdot \mathbf{\Phi}_{fstd}$$

The fluorescence quantum yields ($\mathbf{\Phi}_{fx}$) of the target complexes were determined using the sulfuric acid solution (0.1 mol L^{-1}) of quinine sulfate (1.0 μg mL^{-1}) with a known quantum yield ($\mathbf{\Phi}_{fstd}$ = 0.55) as standard reference at room temperature. where n_x (1.48) and n_{std} (1.34) are the refractive indices of solvents used for the sample and standard. F_x and F_{std} are the areas under the fluorescence curves of the sample and the used standard. A_x and A_{std} are the absorbances of the sample and standard at the excitation wavelength, respectively. The fluorescence quantum yields data of all target complexes are summarized in Table 6.

As shown in the Table 6, the fluorescence quantum yields of the complexes $RE(NO_3)_3L^2 \cdot 2H_2O$ are higher than that of the complexes $RE(NO_3)_3L^1 \cdot 2H_2O$, which is ascribed to the ligands $\mathbf{L^2}$ have an donating electron group (—CH_3) that enlarged the π-conjugated system of the ligands $\mathbf{L^2}$. While the fluorescence quantum yields of the complexes $RE(NO_3)_3L^4 \cdot 2H_2O$ is lower than that of the $RE(NO_3)_3L^1 \cdot 2H_2O$, which is attributed to the chlorine atom caused the electron density of the phenyl ring decreasing and resulted in fluorescence quenching. In addition, the $RE(NO_3)_3L^3 \cdot 2H_2O$ exhibited the lowest quantum yield than that of other target complexes, this is because the energy difference between the triplet state energy level of the ligand $\mathbf{L^3}$ and the lowest excited state level of RE(III) is too small, the energy can back transfer from the rare earth ions to the triplet state energy of the ligands and resulted in the fluorescence quantum yields decreasing. The above results reveal that the 4-position substituted group of benzene ring have a significant effect on the fluorescence quantum yields of the target complexes.

3.7. Electrochemical properties analysis

The electrochemical properties of the target complexes were investigated by means of cyclic voltammetric technique in DMSO solution. The highest occupied molecular orbital (HOMO) and lowest unoccupied molecular orbital (LUMO) energy levels of the target complexes are estimated according to the electrochemical performance and UV absorption spectra [23]. The HOMO and LUMO data for target complexes are obtained by using equation. $E_{HOMO} = -(4.74\ eV + E_{OX})$, $E_{LOMO} = Eg + E_{HUMO}$, $Eg = 1240/\lambda_{onset}(eV)$ [24] (λ_{onset} is the largest UV absorption spectra peak starting value), and their electrochemical data are summarized in Table 7. Because the cyclic voltammograms of all the target complexes are

Table 6
Fluorescence quantum yields data of the target complexes.

Complexes	Absorption wavelength λ/nm	Fluorescence intensity I/a.u.	Fluorescence integral area *F*	Fluorescence quantum yield (*Φ*)
$Eu(NO_3)_3L^1 \cdot 2H_2O$	302	1616	92,518	0.515
$Eu(NO_3)_3L^2 \cdot 2H_2O$	337	595.9	108,935	0.552
$Eu(NO_3)_3L^3 \cdot 2H_2O$	334	232	56,104	0.370
$Eu(NO_3)_3L^4 \cdot 2H_2O$	308	1290	77,017	0.402
$Tb(NO_3)_3L^1 \cdot 2H_2O$	297	2548	84,375	0.517
$Tb(NO_3)_3L^2 \cdot 2H_2O$	300	815.3	70,807	0.593
$Tb(NO_3)_3L^3 \cdot 2H_2O$	286	269.6	57,484	0.311
$Tb(NO_3)_3L^4 \cdot 2H_2O$	335	425	65,191	0.485

Table 7
Electrochemical data for target complexes.

Complexes	λ_{onset} (nm)	Eg (eV)	E_{ox} (v)	E_{HOMO} (eV)	E_{LUMO} (eV)
$Eu(NO_3)_3L^1 \cdot 2H_2O$	259	4.787	0.530	−5.270	−0.483
$Eu(NO_3)_3L^2 \cdot 2H_2O$	261	4.751	0.512	−5.252	−0.501
$Eu(NO_3)_3L^3 \cdot 2H_2O$	262	4.733	0.524	−5.264	−0.531
$Eu(NO_3)_3L^4 \cdot 2H_2O$	262	4.733	0.543	−5.283	−0.550
$Tb(NO_3)_3L^1 \cdot 2H_2O$	259	4.787	0.546	−5.286	−0.499
$Tb(NO_3)_3L^2 \cdot 2H_2O$	260	4.769	0.536	−5.276	−0.507
$Tb(NO_3)_3L^3 \cdot 2H_2O$	263	4.715	0.524	−5.264	−0.549
$Tb(NO_3)_3L^4 \cdot 2H_2O$	262	4.733	0.576	−5.316	−0.583

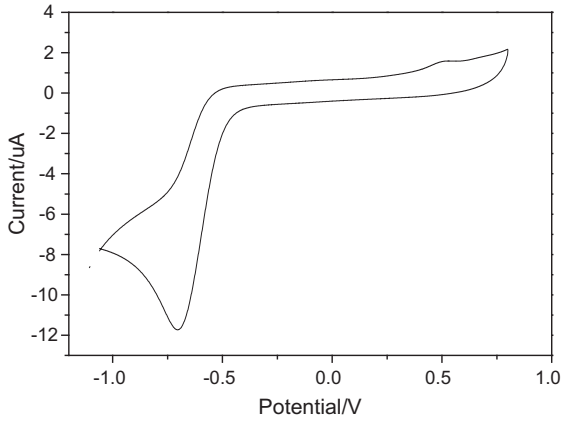

Fig. 9. Cyclic voltammogram of complex $Eu(NO_3)_3\mathbf{L^1} \cdot 2H_2O$.

similar, the cyclic voltammogram of the complex $Eu(NO_3)_3L^1 \cdot 2H_2O$ is selected for illustration and shown in the Fig. 9.

It is seen from the Table 7 that all complexes' oxidation potential occur in the potential range +0.512 to +0.576 V. The energy gap (Eg) of all the target complexes is between 4.715 eV and 4.787 eV. Compared with the one of complexes $RE(NO_3)_3L^1 \cdot 2H_2O$, the HOMO energy levels of complexes $RE(NO_3)_3L^{2-3} \cdot 2H_2O$ are higher, on the contrary, that of the complexes $RE(NO_3)_3L^4 \cdot 2H_2O$ are lower, these phenomena are ascribed to the target complexes with different substituent in the relevant ligands. The results reveal that introduction of donative elecrton group in the ligand can increase the HOMO energy levels of their corresponding complexes, while, introduction of electrophilic group in the ligand can decrease the HOMO energy levels of their corresponding rare earth complexes. Meanwhile, we can observed that the LUMO energy levels of the target complexes are increased in the order of $RE(NO_3)_3L^4 \cdot 2H_2O < RE(NO_3)_3L^3 \cdot 2H_2O < RE(NO_3)_3L^2 \cdot 2H_2O <$. $RE(NO_3)_3L^1 \cdot 2H_2O$.

4. Conclusion

With salicylic acid and hydrazine hydrate as starting material, a series of target 2,5-bis[2′-(substituted phenyl-carbamoyl-methoxy)-phenyl]-l,3,4-oxadiazole were obtained via the reaction of 2,5-Di(o-hydroxyphenyl)-1,3,4-oxadiazole and 2-chloro-N-acetyl-substituted aniline. Their complexes with Eu(III) and Tb(III) were also prepared successfully, and determined by the means of elemental analysis, EDTA titrimetric, molar conductance, UV and FT-IR spectrum as well as thermal performance studies. The luminescence properties of the target complexes were investigated by luminescent spectra, and the results indicate that all complexes show the characteristic luminescence of central ion and the central ions lie in the asymmetry center. The relative fluorescence intensity of the complex with the methyl substituted is the highest than that of other target complexes. The electrochemical properties of the complexes were investigated by cyclic voltammetry, the HOMO energy levels of target complexes substituted by electron-donating group are higher than that of the complexes substituted by electron-withdrawing group. In addition, the thermal analysis provided information about the high thermal stability for the target complexes. In summary, the above results show that the target complexes will be used as the promising candidate luminescent materials.

Acknowledgments

The authors are grateful for the financial support of the National Natural Science Foundation of China (Nos. J1103312 and 21341010), the Innovative Research Team in University (No. IRT1238) and the Science and Technology Project of Hunan provincial Science and Technology Department (No. 2012GK3156). We also thank Dr. William Hickey, the U.S. professor of HRM, for the English editing on this paper.

References

[1] Felipe Gandara, Enrique Gutierrez-Puebla, Marta Iglesias, Natalia Snejko, M. Angeles Monge, [J] Cryst. Growth Des. 10 (2010) 128–134.
[2] Ding Li, Xinya Han, Tu Qidong, Lingling Feng, Wu Di, Yao Sun, Haifeng Chen, Yongjian Li, Yanliang Ren, Jian Wan, [J] Agric. Food Chem. 61 (2013) 7453–7461.
[3] W.X. Li, W.J. Chai, X.J. Sun, T. Ren, X.Y. Shi, J. Fluoresc. 20 (2010) 873–880.
[4] Gerd W. Rabe, Florian A. Riederer, Mei Zhang-Presse, Arnold L. Rheingold, [J] Organomet. 28 (2009) 5277–5280.
[5] M.E.B. Rao, V.G. Rajurkar, Asian J. Chem. 23 (2011) 2648–2652.
[6] Zhao Miao, Xi Peng, Gu Xiaohua, Li Zongren, Gao Mingming, Cheng Bowen, J. Rare Earths 28 (2010) 75–78.
[7] F. Rizzo, F. Meinardi, R. Tubino, R. Pagliarin, G. Dellepiane, A. Papagni, Synth. Met. 159 (2009) 356–360.
[8] J.Q. Bao, C.H. Tang, R.R. Tang, J. Rare Earth 29 (2011) 15–19.
[9] J. Li, L. Zhang, L. Liu, G.F. Liu, J.X. Guo, D.Z. Jia, Inorg. Chim. Acta 360 (2007) 3504–3510.
[10] Wen-Xian Li, Yu-Shan Zheng, Wen-Juan Chai, Tie Ren, Yu Liu, Ying-Jie Li, Xiao-Jun Sun, Gao-Wa Xing, Luminescence 26 (2011) 754–761.
[11] M. Saranga Pani, M. Arjun, D. Sridhar, K. Srinivas, T. Raviprasad, Chin. Chem. Lett. 20 (2009) 909–912.
[12] W.J. Geary, Coord. Chem. Rev. 7 (1971) 81–122.
[13] Sheng-Gui Liu, Rong-Kai Pan, Xiao-Ping Zhou, Xin-Lan Wen, Yi-Zhao Chen, Sheng Wang, Xiao-Bo Shi, Inorg. Chim. Acta 395 (2013) 119–123.
[14] Kai Kong, Haixia Zhang, Ruijun Ma, Yingnan Chen, Haibin Chu, Yongliang Zhao, J. Rare Earths 31 (2013) 32–36.
[15] Bao-Dui Wang, Zheng-Yin Yang, Ding-Wa Zhang, Yan Wang, Spectrochim. Acta Part A 63 (2006) 213–219.
[16] G.C. Xu, L. Zhang, L. Liu, G.F. Liu, D.Z. Jia, Polyhedron 27 (2008) 12–24.
[17] Hongsheng Wang, Xiaoqing Zhao, Mingli Liu, Wei Shi, Peng Cheng, Chin. J. Chem. 30 (2012) 2097–2102.
[18] Liang Tian, Ning Ren, Jian-Jun Zhang, Hong-Mei Liu, Ji-Hai Bai, Hong-Mei Ye, Shu-Jing Sun, Inorg. Chim. Acta 362 (2009) 3388–3394.
[19] Huaqiong Li, Huiduo Xian, Guoliang Zhao, J. Rare Earths 28 (2010) 7–11.
[20] Dongcai Guo, Panliang Wu, Hui Tan, Long Xia, Wenhui Zhou, J. Lumin. 131 (2011) 1272–1276.
[21] G. Vicentini, L.B. Zinner, J. Zukerman-Schpector, K. Zinner, Coord. Chem. Rev. 196 (2000) 353–382.
[22] H.J. Sun, X.T. Fu, H.B. Chu, Y. Du, X.M. Lin, X. Li, Y.L. Zhao, J. Photochem. Photobiol. A 219 (2011) 243–249.
[23] Guoping Ge, Jing He, Haiqing Guo, Fuzhi Wang, Dechun Zou, J. Organomet. Chem. 694 (2009) 3050–3057.
[24] Deqiang Wang, Xiaomei Wang, Qingguo He, Maoyi Zhou, Wenwen Rui, Xutang Tao, Fenglian Bai, Minhua Jiang, Tetrahedron Lett. 49 (2008) 5871–5876.